CHINESE JOURNAL OF GEOCHEMISTRY Vol. 26 No. 1 2007

DOI: 10.1007/s11631-007-0072-0

Simulating experiment on the hydrothermal superimposing metallogenesis of the Dongguashan strata-bound copper deposit

XU Zhaowen (徐兆文)[1*], HUA Ming (华明)[2], LU Xiancai (陆现彩)[1], YANG Xiaonan (杨小男)[1], RAO Bing (饶冰)[1], WANG Yunjian (王云建)[1], JIANG Shaoyong (蒋少涌)[1], LU Jianjun (陆建军)[1], NIE Guiping (聂桂平)[2], and HUANG Shunsheng (黄顺生)[2]

[1] *The State Key Laboratory of Mineral Deposit Research, Department of Earth Sciences, Nanjing University, Nanjing 210093, China*

[2] *Geological Survey of Jiangsu Province, Nanjing 210018, China*

* *Corresponding author, E-mail: tzb@nju.edu.cn*

Received January 9, 2006; accepted April 25, 2006

Abstract Series of sedimentary hydrothermal-diplogenetic copper deposits have been found scattering in the region along the middle-lower reaches of the Yangtze River, and their metallogenetic mechanism is still in hot debate. In order to reveal the ore-forming kinetics of sedimentary process and hydrothermal superimposition, and evaluate the role of sedimentary pyrite in the enrichment and precipitation of copper, a set of simulating experiments on the reaction between pyrite and $CuCl_2$ solution were conducted. According to the physicochemical characteristics of the ore-forming fluid of the Dongguashan copper deposit, Anhui Province, 100 MPa was selected as the experimental pressure, and the experimental temperatures were set at 450, 350, 250 and 150°C, respectively. The reactions between pyrite grains isolated from the Shimenkou strata-bound pyrite deposit and the solution with 0.2 mol/L $CuCl_2$ and 1.0 mol/L NaCl were experimentally simulated. Then, variations in surface topography and surface chemistry of the experimental pyrite grains were documented using scanning electronic microscopy (SEM), atomic force microscopy (AFM), Auger electron spectrometry (AES) and X-ray photoelectron spectroscopy (XPS), and the solution and newly formed minerals were analyzed using inductively coupled plasma (ICP-AES) and X-ray diffraction (XRD) techniques. Desulphurization of pyrite surface was observed and new copper minerals were detected. It is proposed that pyrite can act as a geochemical barrier for the enrichment and precipitation of copper from the solution under the experimental conditions. Furthermore, the ore-forming mechanism of sedimentary hydrothermal-diplogenetic copper deposits was discussed.

Key words pyrite; hydrothermal-diplogenetic copper deposit; surface mineral; geochemical barrier; experimental simulation; Dongguashan copper deposit

1 Introduction

The region along the middle-lower reaches of the Yangtze River is an important mineralizing belt of Fe, Cu, Au, S and so on, with a series of sedimentary-hydrothermal diplogenetic mineral deposits (Xu Keqin and Zhu Jinchu, 1978; Liu Yuqing et al., 1984; Gu Lianxing and Xu Keqin, 1986; Zhai Yusheng et al., 1992; Gu Lianxing et al., 1993; Wang Xiuzhang et al., 1998; Du Yangsong, 1999; Gu Lianxing et al., 2000; Xu Zhaowen et al., 2005). Some geologists thought that Carboniferous massive sulfide exhalative sediments were the basis for the late diplogenetic mineralization (Gu Lianxing and Xu Keqin, 1986; Gu Lianxing et al., 1993; Gu Lianxing et al., 2000; Xu Zhaowen et al., 2005). Although there have been still diverse viewpoints on the mineralization mechanisms, the widely distributed stratified ore-bodies in this region are thought to be the product of superimposition of magmatic hydrothermal fluids on Carboniferous exhalation sediments during the Yanshanian period based on detailed orefield geology, fluid geochemistry, isotope geochemistry and ore petrology studies (Xu Zhaowen et al., 2000; Lu Jianjun et al., 2003; Xu Zhaowen et al., 2005). Besides these geological and geochemical studies, only a few experimental studies on the mineralization mechanism have been reported. Wu Xueyi et al. (1995) experimentally simulated the

structural controls on the mineralization, and Chen Jun et al. (1989) carried out a series of experiments on the mineralization of sedimentary hydrothermal-diplogenetic tin deposits. On the issue of the migration, enrichment, precipitation and mineralization of copper, most experiments were designed as the Cu-Fe-S-H_2O-NaCl solution system under relatively low pressures and temperatures (Zhao Bin et al., 1995; Tan Kaixuan and Zhang Zheru, 1994; Tan Kaixuan et al., 1996; Creerar and Barnes, 1976; Cowper and Richard, 1989; Ellis and Giggenbach, 1971; Helgeson, 1969; Louis, 1973; Barton, 1973), which are quite different from the geological facts. In order to disclose the metallogenesis of these important deposits, the authors designed and carried out a series of simulating experiments on copper mineralization in the pyrite-$CuCl_2$-NaCl system according to the measured physical-chemical properties of ore-forming fluids from the Dongguashan sedimentary-hydrothermal diplogenetic ore deposits.

2 Samples and experiments

2.1 Preparation of pyrite sample and solution

Pyrite samples were collected from the sedimentary stratiform pyrite orebodies in –35 m-deep gallery at the western Shimenkou working section, Qingyang County, Anhui Province, which are the same as the exhalation sediments at Dongguashan. The ores were crushed as fine as powder ranging from 500 to 180 μm in diameter, and then the pyrite grains were picked up under microscope. Coarse grains (500 μm in size) and fine powder (180 μm in size) were prepared for surface observation and enhancing the reaction rates, respectively. The selected bigger grains are present in the form of perfect cubic crystals. Both pyrite grains were sealed and kept for experiments after ultrasonic cleaning and vacuum drying.

Liu Weihua et al. (2001), Matthew et al. (2000) and Xiao Zhifeng et al. (1998) experimentally studied the occurrence of copper in the ore-forming fluid. According to Matthew et al. (2000), copper is present mainly as $CuCl_x^{2-x}$ complex (where x ranges from 1.0 to 4.0 depending on the pressure and temperature) in Cl^- rich solution. According to the measured temperature and pressure of the fluid inclusions from the Donggguashan copper deposit, as reported by Huang Shunsheng et al. (2003) and Xu Zhaowen et al. (2003), 0.2 mol/L $CuCl_2$ and 1.0 mol/L NaCl solutions were freshly prepared before experiments. Distilled water was used, and both $CuCl_2$ and NaCl were chemically pure.

2.2 Experimental simulation

Experimental simulations were carried out using a high-pressure-temperature rapid quench vessel (RQV) at the State Key Lab for Mineral Deposit Research. Five parallel simulations were designed. The experimental temperatures were set at 450, 350, 250 and 150ºC respectively, and the pressure was 100 MPa. All the experiments continued for 5 days. In each of the simulations, 0.6100±0.100 g $CuCl_2$ solution and 0.2000±0.0050 g pyrite, including one coarse pyrite grain, were sealed in a gold tubular bag and then the bag was put into the autoclave. The pressures were measured using a tubular spring pressure gauge, and the experiment temperatures were determined on an RPK-103 Pt-Rh thermocouple after calibration on a UJ3 potentiometer. The errors involved in the pressure and temperature measurements are ±5 MPa and ±2ºC, respectively. The temperature programming was controlled by an XTMA-1000 digital director. As each experiment was finished, the autoclave was rotated from the horizontal state to the obsequent vertical state, and then the sample bag fell into the quencher vessel. After several seconds of quenching, the cooled bag was opened and the solid minerals and precipitates were isolated from the solution. Both the solid separates and solution were sealed for further chemical analysis and microscopic observation.

3 Precipitation and reacted pyrite

At first, the solid separates were roughly examined under optical microscope. The precipitates were clearly displayed on the surfaces of coarse pyrite grains involved in reactions at 450, 250 and 150ºC, respectively. The pyrite powder was aggregated together and mixed with blue sheet-like precipitates. Recystallization phenomena were also observed in the aggregates.

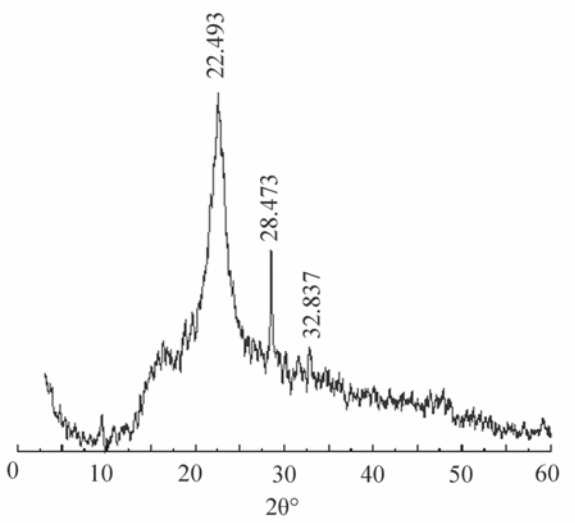

Fig. 1. XRD spectra of blue precipitates.

3.1 X-ray diffraction (XRD)

The blue precipitate was analyzed using an X-ray diffractometer (X'TRA, Switzerland). The spectrum is shown in Fig. 1. It is demonstrated that the precipitate is covellite (CuS).

3.2 Scanning electron microscopy (SEM)

The morphological characteristics of pyrite crystals before and after experiments were observed under a scanning electron microscopy (SEM, Hitachi S-650), and the surface composition of the pyrite crystals was analyzed by energy-dispersive X-ray analysis (EDAX). The samples were sputter-coated with Au for 90 sec. before observation. An accelerating voltage of 20 kV was used. The data were collected for 200 sec., and the sensitivity was 2‰. The SEM images and chemical composition of the surface of pyrite grains used in the experiments is shown in Fig. 2 and is presented in Table 1, respectively.

Both the spot analysis (spot a) and surface analysis (area I) indicated that the pristine pyrite grains are chemically composed of FeS_2 with trace copper mixture of 0.16 wt% (Fig. 2A). Some irregular precipitates and many cubic microcrystals emerged on the surface of the pyrite crystals involved in reactions at 150ºC (Fig. 2B). The spot analysis indicated that the irregular precipitates contain about 7.0 wt% copper and the microcrystals contain 19.23 wt% copper, whereas no copper was detected on the surface of the reacted pyrite. The surface composition was determined to be Fe_7S_8, and the microcrystals must be a type of copper mineral. While the reaction temperature increased to 250ºC, two types of precipitates, tabular and sheet-like microcrystals, occurred on different crystal faces (Fig. 2C, D). The tabular precipitates have higher copper contents than the sheet-like ones. As shown by the analysis results (spots c and d in Table 1), their chemical formulas are (Cu, $Fe)_9S_5$ and Cu_9S_8, corresponding to alpha-chalcocite and yarrowit, respectively. In addition, the sulfur contents of the pyrite surface decreased continuously. As the reaction temperature increased to 350ºC, no precipitation on the pyrite surface was observed, and the sulfur contents of the pyrite surface were reduced to 42.31% (Table 1). But many crystal grains were precipitated on the surface of the pyrite involved in reactions at 450ºC (Fig. 2F). The energy spectral analysis showed that the crystalline precipitates may be bornite, Cu_5FeS_4 (spots e, f), and the surface analysis of area VI indicated that the composition is chalcopyrite (Fig. 2F and Table 1).

Table 1. X-ray energy spectrometric analyses coupled with SEM data

Spot analysis	Element	wt%	atom.%	Rel. error	ZAF	Surface analysis	Element	wt%	atom.%	Rel. error	ZAF
a (Pristine)	Cu	0.16	0.11	12.92	1.18	I (Pristine)	Cu	0.04	0.03	25.84	1.18
	Fe	48.81	35.41	0.56	1.09		Fe	47.79	34.29	0.56	1.09
	S	51.03	64.49	0.41	1.23		S	52.17	66.69	0.41	1.23
b (150ºC)	Cu	7.00	4.60	2.38	1.17	II (150ºC)	Cu	19.23	13.09	1.18	1.14
	Fe	46.49	34.78	0.69	1.08		Fe	38.33	29.68	0.63	1.06
	S	46.51	60.62	0.52	1.27		S	42.44	57.24	0.47	1.33
c (250ºC)	Cu	75.65	62.08	0.63	1.04	III (150ºC)	Cu	–	–	–	–
	Fe	2.43	2.27	2.60	0.93		Fe	60.28	46.56	0.59	1.07
	S	21.92	35.65	0.76	1.48		S	39.72	53.44	0.56	1.28
d (250ºC)	Cu	68.55	53.60	0.69	1.06	IV (250ºC)	Cu	0.12	0.08	17.95	1.17
	Fe	3.51	3.13	1.30	0.95		Fe	52.50	38.85	0.64	1.08
	S	27.93	43.28	0.70	1.44		S	47.38	61.07	0.49	1.20
e (450ºC)	Cu	64.96	51.80	0.67	1.06	V (350ºC)	Cu	0.16	0.11	18.07	1.16
	Fe	10.70	9.71	1.24	0.96		Fe	57.53	43.79	0.72	1.07
	S	24.35	38.49	0.70	1.44		S	42.31	56.10	0.63	1.22
f (450ºC)	Cu	61.42	48.19	1.32	1.06	VI (450ºC)	Cu	33.15	24.13	1.07	1.11
	Fe	12.37	11.04	2.21	0.96		Fe	33.74	27.96	0.80	1.02
	S	26.21	40.77	1.31	1.34		S	32.53	46.95	0.65	1.34

Note: The analysis was carried out in the Mordern Analysis Center of Nanjing University. ZAF represents the integrated correction of atomic correction, absorbing correction and fluorescence correction. Spot a, b, c, d, e, f and area I, II, III, IV, V and VI are shown in Fig. 2; – not detected.

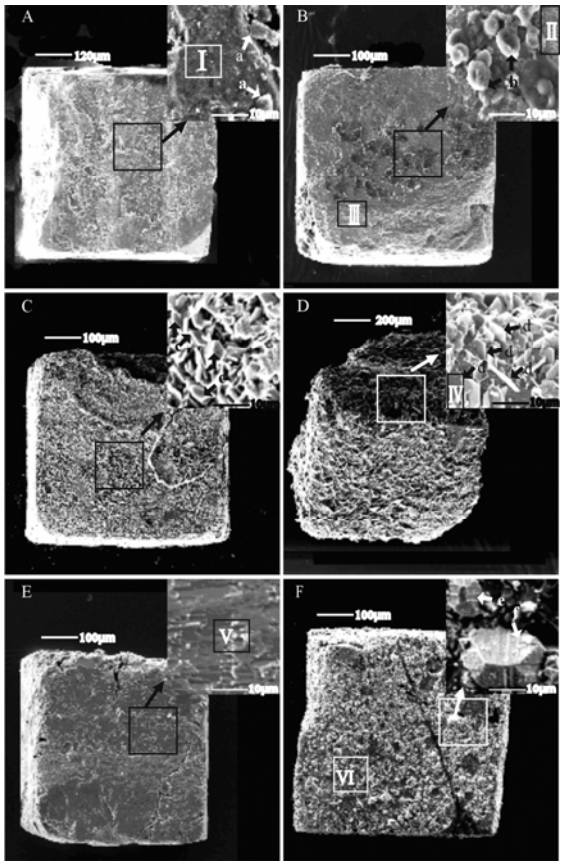

Fig. 2. SEM images of pyrite samples before and after reactions. A. Pristine pyrite; B. pyrite involved in reaction at 150ºC; C and D. pyrite involved in reaction at 250ºC; E and F. pyrite involved in reaction at 350ºC and 450 ºC. I, II, III, IV, V and VI are the areas for surface analysis; a, b, c, d, e and f are the points for spot analysis.

3.3 Atomic force microscopy (AFM)

In order to disclose the surface morphological characteristics of the reacted pyrite, the crystal faces of the pyrite before and after reactions were observed under atomic force microscopy (AFM) (Digital Instruments, Nanoscope IIIa Model) at room temperature. Contact mode and J-type piezoquartz scanning tube were employed, and the scanning frequency is 2 Hz. Figure 3 shows the AFM images of the experimental pyrite before and after reactions, and Figure 4 displays the micromorphological profiles of the pyrites. The crystal faces of the pristine pyrite are rough, and many particulates measured at about 50 nm are adhered on the surface. Some newly formed cubic and rhombohedron crystals, which are deduced as the copper-bearing microcrystals found in SEM images, are observed on the surface of pyrite involved in reaction at 150ºC. These crystals are about 3.5 μm in diameter, and about 250 nm in length. As the reaction temperature increased to 350ºC, orientated humping morphological features occurred on the pyrite surface (Fig. 3C). The precipitates are 15 nm long. Furthermore, growth steps are found on the surface of the pyrite involved in reaction at 450ºC, and their heights vary from 3 to 25 nm.

3.4 X-ray photoelectron spectrography (XPS)

XPS is a reliable method to constrain the chemical composition of mineral surface. The XPS data were obtained with a PHI-550 type photoelectron spectrograph. The Al*K*α radiation was employed as the lamp source, and the operating voltage and electricity were 9.5 kV and 30 mA, respectively. The energy streams for wide and narrow scanning were set at 100 keV and 500 keV, respectively. All the peak locations were standardized according to the Cls bonding energy, and the quantitative analysis of those elements was conducted based on the peak areas and sensitivity factors.

The S/Fe atomic ratio of the pristine pyrite surface was exactly 2∶1, and no copper was detected; the S/Fe changes and copper deposition were detected on the reacted pyrite surface (Table 2). The Cu/Σ ratios varied sharply with reaction temperature. Cu/Σ ratios for the pyrite surface involved in reactions at

Table 2. Results of wide scanning XPS analysis of pyrite before and after the experiments (At.%)

Sample	Temperature (ºC)	Atomic ratio						General parameter			
		C	O	N	S	Fe	Cu	S/Σ	Fe/Σ	Cu/Σ	S:Fe
10	450	69.91	11.72	1.79	5.77	5.59	4.38	0.37	0.35	0.28	1.03
11	350	64.67	9.22	4.21	8.51	11.31	1.96	0.39	0.52	0.09	0.75
12	250	49.65	18.59	4.58	8.45	2.85	15.86	0.31	0.11	0.58	2.96
13	150	57.31	15.23	6.79	8.36	8.50	3.77	0.41	0.41	0.18	0.98
Pristine		64.99	15.26	0.64	11.25	5.75	–	–	–	–	1.98

Note: Note: Analyzed at the Research Institute of Nanjing Chemical Industry Group; C, O and N are the contaminants of the surficially adsorbed air; Σ=S+Fe+Cu; – not detected.

Fig. 3. Surface micromorphology of the pyrite before and after the experiments. A. Pristine pyrite; B, C, D. pyrite involved in reactions at 150, 350 and 450ºC; E. amplificatory of part of B; F. amplificatory of part of D.

150, 250, 350 and 450ºC respectively were 0.18, 0.58, 0.09 and 0.28, respectively, suggesting various copper-bearing deposits occurred on the crystal faces of the reacted pyrites.

3.5 Auger electron spectrometry (AES)

AES was employed to compare the chemical profiles of pyrites before and after experimental simulations in this study. The Ar ion gun with an operation voltage of 4 kV and electric current of 15 mA was used to spatter the pyrite crystal faces. The spattering angle was set at 45º, the spattering rate was 2 nm/min and the scanning area was 2 mm × 2 mm. The spattering duration was selected as 2100 sed. Because pyrite surface is sensitive to air pollution, the contents of carbon and oxygen in the pyrite surface are generally high (Table 2) (Michael and Hochella, 1988; Nesbitt and Muir, 1994). In this study, the contents of carbon and oxygen were eliminated and the measured AES data were normalized to 100%, as is listed in Table 2, and the corresponding chemical profiles are shown in Fig. 5. Sulfur, iron and copper tend to vary with spattering depth evidently and

Fig. 4. Surface micromorphological profile of the reacted pyrite. a, b, c and d represent the profiles of the left images of A, B, C and D.

reaction temperature (Fig. 5), especially in the surficial layer at the 15-nm depth. Although the copper contents are variable, a type of copper-rich layers with a thickness of about 50 nm is shown in the pyrite surface involved in reactions at the four temperatures. The highest copper content was found in the reacted pyrite at 250ºC, and the lowest at 350ºC, which are in good consistency with the XPS analysis

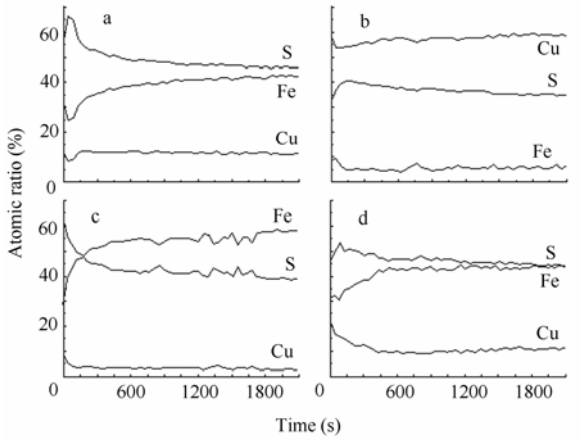

Fig. 5. AES chemical profiles of crystalline faces of the reacted pyrite. a, b, c and d represent the experimental pyrites reacted at 150ºC, 250ºC, 350ºC and 450ºC, respectively.

data. Copper-rich precipitates were only found in the pyrite with the surficial layer having the highest copper content. It is deduced that the copper mainly occur as copper-bearing minerals on the reacted pyrite surfaces.

4 Discussion

It is clearly indicated that the surface chemical properties of the pyrites involved in reactions at different temperatures are quite different. There are irregular precipitates and dissolved pits occurring on the pyrite surfaces involved in reaction at 150ºC, which suggests there have been both precipitation and dissolution on the pyrite surface. The regular crystalline precipitates occurring on the pyrite involved in reaction at 250ºC have the highest copper content. But the orientated humping morphological characteristics at 350ºC and the growth steps at 450ºC occurring on the reacted pyrites (Fig. 3) may suggest the pyrite surface dissolution is accompanied with the formation of precipitates at high temperatures and pressures. On the other hand, the contents of sulfur and iron in the pyrite surface tend to decrease drastically with increasing reaction temperature (Table 1). Furthermore, the high concentrations of iron and zinc, about several thousand 10^{-6}, were detected in the reacting fluid. All the experimental results proved that the pyrite had experienced a complex process, i.e., mixing, partial dissolution and deposition of copper-bearing minerals. Such phenomena were also found in various ore deposits. Copper, zinc and iron in the massive sulfide deposits could be remobilized, transported as chloric complexes, and then precipitated as copper sulfides in the belts with a mineral assemblage of pyrite and pyrrhotite, which considerably improved the grade of the primary ore bed (Zaw et al., 1999). Halbach et al. (1998) observed a mineral association of bornite, chalcopyrite and alphachalcocite growing around the primary pyrite in the massive sulfide ore, which is the product of hydrothermal-diplogenetic process in the late stage. In the Dongguashan copper deposit, Lu Jianjun et al. (2003) also found similar rapakivi texture, in which the preexisting pyrite was surrounded by chalcopyrite.

The precipitation of alohachalcocite and yarrowit on the pyrite surface involved in reaction at 250ºC may be mixed the exchangement of the iron atom in pyrite surface by copper from experimental fluid. Cowper et al. (1989) found that the diffusion and exchange of S, Cu and Fe played an important role in the reaction between pyrrhotite and $CuSO_4$ solution, in which a series of copper sulfides with varying Cu contents were formed. Of course, the non-linear relations between Fe and Cu on the pyrite surface, as shown by AES, suggests that the Fe-Cu exchange is not the dominant mechanism. It is quite different from the conclusion of exchangement made by Wu Daqing et al. (1996) based on the experiments on the reaction between sulfide and metal ions under low temperature and atmospheric pressure. In our experiments, the thermodynamic condition controlled the reaction processes. Although a copper-rich layer was revealed by the XPS and AES data, no certain precipitate was found on the pyrite involved in reaction at 350ºC , as observed in the SEM images, which may be attributed to the high activity of S^{2-} in the Cu-Fe-S-H_2O system and the properties of crystal faces at 350ºC. The deposition of covellite and the decrease of sulfur contents on the pyrite surface involved in reactions at 450, 350 and 250 ºC suggested that the dissociative sulfur derived from desulfization of pyrite reacted with the copper ions in fluid, then leading to the precipitation of covellite under high temperature and pressure. In other words, covellite could be formed as a result of thermal alteration of sedimentary pyrite, and this situation is similar to what was encountered in the Dongguashan deposit (Gu Lianxing, 1999).

The inductively coupled plasma (ICP-AES) analysis of the experimental fluid showed that the release amounts of trace metals from pyrite vary by 2–3 orders of magnitude. It is suggested that the difference in occurrence of metals in the pyrite controls their releasing rates. According to the occurrence, Huston et al. (1995) grouped the trace metals in the pyrite into three associations, including metals that were captured in inclusions (Cu, Zn, Pb and Bi), stoichiometrically and nonstoichiometrically substituted metals of Fe and S. Non-stoichiometrically substituted elements include As, Tl, Au and Mo, and stoichiometrically substituted ones include Co and Ni which substituted Fe, Se and Te which substituted S. The release amount of a special element also varied with experimental pressure and temperature, which stands on the control of physicochemical conditions on the hydrothermal alteration. This finding can explain the difference in arsenic contents of sulfide minerals between the Shimenkou deposit and the Dongguashan deposit. The As contents of the Shimenkou deposit are one order of magnitude higher, and the patterns of S/Se and Co/Ni vary more regularly than those of the Dongguashan deposit (Xu Zhaowen et al., 2006). This diversity can be attributed to the extent of hydrothermal alteration.

5 Conclusions

(1) The sulfur released from the pyrite surface reacting with $CuCl_2$-bearing brine under high pressure and temperature was analyzed in this study. It has been proved that thermal geofluids could alternate the original textures of sedimentary ore bodies.

(2) The various copper sulfides, precipitated on the crystal faces of pyrites, resulted from the reaction between sulfur and iron released from pyrite and copper in fluid, suggesting that the sedimentary pyrite played a role as geochemical barriers in the enrichment of ore-forming elements.

(3) The leaching behaviors of Zn, Pb, Bi, Co, Ni, As and Cu from pyrites in hydrothermal fluids depend on the temperature, pressure and other physicochemical conditions. This finding provides experimental evidence for the remobilization of ore-forming elements in sedimentary-hydrothermal diplogenetic processes.

(4) Differences in the copper-bearing precipitates, dissolution rate of pyrite and remobilization of trace elements caused by differences in reaction temperature and pressure indicate that physicochemical conditions can control the geochemical behavior of the pyrite-$CuCl_2$ brine system.

Acknowledgements This work is supported by the National Natural Science Foundation of China (No. 49873016) and the Ph. D Program Foundation of Education of China (Nos. 20020284035, 20050284043).

References

Barton P.B. Jr. (1973) Solid solutions in the system Cu-Fe-S. Part I: the Cu-S and CuFe-S joins [J]. *Economic Geology.* **68**, 455–465.

Chen Jun, Zhou Huaiyang, Wu Houze, and Zeng Jiliang. (1989) Ore-forming simulating experiments of Dachang strata-bound Tin deposits, Guangxi [J]. *Journal of Guilin College of Geology.* **9**, 380–386 (in Chinese with English abstract)

Cowper M. and Rickard D. (1989) Mechanism of chalcopyrite formation from iron monosulphide in aqueous solutions (<100ºC, pH 2–4.5) [J]. *Chemical Geology.* **78**, 325–341.

Creerar D.A. and Barnes H.L. (1976) Ore solution chemistry, V. Solubilities of chalcopyrite and chalcocite assemblages in hydrothermal solution at 200ºC to 350ºC [J]. *Economic Geology.* **71**, 772–794.

Du Yangsong (1999) Petrological and mineralogical study of enclaves in plutons in the typical mining districts of Tongling, Anhui and metallogeny [J]. *Chinese Journal of Geochemistry*. **18**, 208–218.

Ellis A.J. and Giggenbach W. (1971) Hydrogen sulphide ionization and sulphur hydrolysis in high temperature solution [J]. *Gechimica et Cosmochimica Acta.* **35**, 247–260.

Gu Lianxing (1999) Advances in research on massive sulfide deposits: A review [J]. *Geological Review.* **45**, 265–275 (in Chinese with English abstract).

Gu Lianxing and Xu Keqin (1986) On the Carboniferous submarine massive sulphide deposits in the lower reaches of the Changjiang River [J]. *Acta Geologica Sinica.* **5**, 176–188 (in Chinese with English abstract).

Gu Lianxing, Hu Wenxuan, He Jinxiang, and Xu Yaotong (1993) *Geology and Genesis of the Upper Paleozoic Massive Sulphide Deposits in South China* [M]. pp.83–96. Transactions of Institution of Mining and Metallurgy (Section B: Applied Earth Science).

Gu Lianxing, Hu Wenxuan, He Jinxiang, Ni Pei, and Xu Keqin (2000) Regional variations in ore composition and fluid features of massive sulphide deposits in South China: Implications for genetic modeling [J]. *Episodes.* **23**, 110–118.

Halbach P., Blum N., Munch U., Pluger W., Garbe-Schonberg D., and Zimmer M. (1998) Formation and decay of a modern massive sulfide deposit in the Indian Ocean [J]. *Mineralium Deposita.* **33**, 302–309.

Helgeson H.C. (1969) Thermodynamics of hydrothermal systems at elevated temperatures and pressures [J]. *Am. Jour. Sci.* **267**, 729–804.

Huang Shunsheng, Xu Zhaowen, and Ni Pei (2003) Inclusion geochemistry of Dongguashan hydrothermal superimposion copper deposit in the Tongling area, Anhui [J]. *Contributions to Geology and Mineral Resources Research.* **18**, 34–38 (in Chinese with English abstract).

Huston D.L., Sie S.H., Suter G.F., Cooke R.D., and Both A.R. (1995) Trace elements in sulfide minerals from Eastern Australian volcanic-hosted massive sulfide deposits: Part I. Poton microprobe analyses of pyrite, chalcopyrite, and sphalerite, and Part II. Selenium levels in pyrite: Comparison with $\delta^{34}S$ values and implicated for the source of sulfur in volcanogenic hydrothermal systems [J]. *Economic Geology.* **19**, 1167–1196.

Liu Weihua, Mcphail D.C., and Joel Brugger (2001) An experimental study of copper(I)-chloride and copper(I)-acetate complexing in hydrothermal solution between 50ºC and 250ºC and vapor-saturated pressure [J]. *Geochimica et Cosmochimica Acta.* **65**, 2937–2948.

Liu Yuqing, Liu Zhaolian, and Yang Chengxing (1984) Stable isotope studies of the Dongguashan copper deposit in Tongling Prefecture, Anhui Province [J]. *Bull. Institute of Mineral Deposits. **CAGS***. (1), 70–101 (in Chinese with English abstract).

Louis J.C. (1973) New data on phase relations in the Cu-Fe-S system [J]. *Economic Geology.* **68**, 443–454.

Lu Jianjun, Hua Renmin, Xu Zhaowen, Gao Jianfeng, and Li Juan (2003) A two-stage model for formation of the Dongguashan Cu-Au deposit [J]. *Geological Journal of China Universities.* **9**, 678–690 (in Chinese with English abstract).

Matthew D. Collings, David M. Sherman, and K. Vala Ragnarsdottir (2000) Complexions of Cu^{2+} in oxidized NaCl brines 25ºC to 175ºC: Results from *in-situ* EXAFS spectroscopy [J]. *Chemical Geology.* **167**, 65–73.

Michael F. and Hochella Jr. (1988) Sputter depth profiling in mineral-surface analysis [J]. *American Mineralogist.* **73**, 1449–1456.

Nesbitt H.W and Muir I.J. (1994) X-ray photoelectron spectroscopic study of pristine pyrite surface reacted with water vapour and air [J]. *Geochimica et Cosmochimica Acta.* **58**, 4667–4679.

Tan Kaixuan and Zhang Zheru (1994) Soluble dynamics of chalcocite, chalcopyrite and bornite in 2 mol/L NaCl solution [J]. *Chinese Science Bulletin.* **39**, 2165–2168 (in Chinese).

Tan Kaixuan, Zhang Zheru, and Wang Zhonggang (1996) The chemical oscillations and chaotic attractors of soluble reaction of chalcopyrite in NaCl solution [J]. *Chinese Science Bulletin.* **41**, 720–721 (in Chinese with English abstract).

Wang Xiuzhang, Cheng Jingping, Mo Cehui, Liang Huaying, Xia Ping, and Shan Qiang (1998) Geology and geochemistry of reworking gold deposits in intrusive rocks of China—II. Gold deposits and their genesis [J]. *Chinese Journal of Geochemistry*. **17**, 193–200.

Wu Daqing, Peng Jinlian, and Chen Guoxi (1996) Experimental study on

adsorption of metal ions onto sulfides (Ⅰ): Types [J]. *Geochimica.* **25**, 181–189 (in Chinese with English abstract).

Wu Xueyi, Yang Yuangen, Wang Zijiang, Li Jinming, and Wang Changsheng (1995) Geological and geochemical characteristics of the Ashele copper deposit, Xinjiang [J]. *Acta Mineralogica Sinica.* **15**, 199–204 (in Chinese with English abstract).

Xiao Zhifeng, Gammons C.H., and Wiliams Jones A.E. (1998) Experimental study of copper (I) chloride complexing in hydrothermal solutions at 40 to 300ºC and saturated water vapor pressure [J]. *Geochimica et Cosmochimica Acta.* **62**, 2949–2964.

Xu Keqin and Zhu Jinchu (1978) Origin of sedimentary-(or volcanosedimentary-) iron-copper deposits in some fault depression belts in Southeast China [J]. *Fujian Geology.* **4**, 1–68 (in Chinese with English abstract).

Xu Zhaowen, Fang Changquan, Lu Xiancai, Jiang Shaoyong, Gao Geng, Yang Xiaonan, Ni Guiping, Zhu Shipeng, and Hua Ming (2006) Study of stratied pyretic deposit geological characteristics and genesis in Shimenkou [J]. *Contributions to Geology and Mineral Resources Research.* **20**, 10–14 (in Chinese with English abstract).

Xu Zhaowen, Lu Jianjun, Lu Xiancai, Gao Jianfeng, Liu Suming, Luo Qingchun, and Jiang Zhangping (2000) Geological characteristics and genesis of Cu-Au mineral Shizishan Deposit in Tongling, Anhui Province [J]. *Bulletin of Mineralogy, Petrology and Geochemistry.* **19**, 233–234 (in Chinese with English abstract).

Xu Zhaowen, Lu Xiancai , Ling Hongfei, Lu Jianjun, Jiang Shoyong, Nie Guiping, Huang Shunsheng, and Hua Ming (2005) Metallogenetic study and age determination of diplogenetic mineralization of Dongguashan stratified copper deposit, Anhui Province [J]. *Acta Geologica Sinica* (English Edition). **79**, 405–413.

Xu Zhaowen, Lu Xiancai, Huang Shunsheng, Ni Pei, Hua Ming, and Lu Jianjun (2003) Characteristics and evolution of ore-forming fluid in Dongguashan copper deposit, Anhui province, China [J]. *Geochimica et Cosmochimica Acta*. **67**(suppl.), A542.

Zaw Khin, Huston D.L., and Large R.R. (1999) A chemical model for the Devonian remobilization process in the Cambrian volcanic-hosted massive sulfide Rosebery deposit, Western Tasmania [J]. *Economic Geology.* **94**, 529–545.

Zhai Yusheng, Yao Shuzhen, Lin Xinduo, Zhou Xunruo, and Wan Tianfeng (1992) *The Genesis of Copper-Iron (Gold) Deposits of Middle-Lower Yangtze Area* [M]. pp.1–235. Geological Publishing House, Beijing (in Chinese).

Zhao Bin, Wang Shengyuan, Wu Houze, and Liu Zhengyi (1995) *High Temperature and High Pressure Experimental Geochemistry* [M]. pp.75–101. Science Press, Beijing (in Chinese).